

Coordination field analysis of the fluorescence spectra of  $\text{LaOX:Er}^{3+}$  phosphors ( $X^-$  identical to  $\text{Cl}^-$ ,  $\text{Br}^-$ )

This content has been downloaded from IOPscience. Please scroll down to see the full text.

1991 J. Phys.: Condens. Matter 3 483

(<http://iopscience.iop.org/0953-8984/3/4/011>)

View [the table of contents for this issue](#), or go to the [journal homepage](#) for more

Download details:

IP Address: 218.26.34.64

This content was downloaded on 25/10/2014 at 13:14

Please note that [terms and conditions apply](#).

## Coordination field analysis of the fluorescence spectra of LaOX:Er<sup>3+</sup> phosphors (X<sup>-</sup> ≡ Cl<sup>-</sup>, Br<sup>-</sup>)

Yang Pin<sup>†</sup>, Li Sidian<sup>‡</sup> and Wang Yuekui<sup>†</sup>

<sup>†</sup> Institute of Molecular Science, Shanxi University, Taiyuan, People's Republic of China

<sup>‡</sup> Department of Chemistry, Yuncheng Teachers' College, Yuncheng, People's Republic of China

Received 11 April 1990, in final form 14 September 1990

**Abstract.** LaOX:Er<sup>3+</sup> phosphors (X<sup>-</sup> ≡ Cl<sup>-</sup>, Br<sup>-</sup>) were synthesized and their fluorescence spectra at room and liquid-nitrogen temperature measured. Based on the double-sphere coordination point-charge field model, the coordination field perturbation energy levels of Er<sup>3+</sup> ions doped in LaOX matrices were calculated and the corresponding spectra assigned. The energy levels calculated agree well with the spectra observed, and the theoretical assignments give a reasonable explanation for the temperature effect on the <sup>4</sup>I<sub>15/2</sub> → <sup>4</sup>F<sub>3/2,7/2</sub> excitation bands. A comparison of the coordination field parameters B<sub>q</sub><sup>k</sup> for the whole LaOX:Er<sup>3+</sup> (X<sup>-</sup> ≡ Cl<sup>-</sup>, Br<sup>-</sup>) and LaOX:Eu<sup>3+</sup> (X<sup>-</sup> ≡ Cl<sup>-</sup>, Br<sup>-</sup>, I<sup>-</sup>) series shows an increase in the strength of the coordination field effect with the increasing ionic radius and electronegativity of X<sup>-</sup> host anions.

### 1. Introduction

The PbFCl-type phosphors REOX and MFX activated with trivalent and divalent rare-earth (RE) ions are both excellent x-ray and photostimulated luminescence materials. Considerable attention has been paid to the study of the spectra and electronic energy levels involving coordination field (CF) perturbation on RE ions in these matrices. REOX compounds offer an excellent opportunity to observe the variation in the CF effect in both the RE and the halide series. Hölsä *et al* [1] studied the CF effect on Eu<sup>3+</sup> and Tb<sup>3+</sup> in REOX by fitting the spectra phenomenologically, but they did not involve the spectral analyses of other RE ions. In our previous work [2], this study was extended to LaOX:Pr<sup>3+</sup> and LaOX:Dy<sup>3+</sup> based on the double-sphere coordination point-charge field (DSCPCF) model [3]. In this paper, the results for LaOX:Er<sup>3+</sup> will be reported.

The excitation and emission spectra of Er<sup>3+</sup> in crystals are typical f–f transitions. It has four characteristic emission bands for transitions between excited states and the ground state: green band (<sup>4</sup>S<sub>3/2</sub> → <sup>4</sup>I<sub>15/2</sub>), red band (<sup>4</sup>F<sub>9/2</sub> → <sup>4</sup>I<sub>15/2</sub>), IR1 (<sup>4</sup>I<sub>11/2</sub> → <sup>4</sup>I<sub>15/2</sub>) and IR2 (<sup>4</sup>I<sub>13/2</sub> → <sup>4</sup>I<sub>15/2</sub>). Excited with red light, the <sup>4</sup>I<sub>9/2</sub> → <sup>4</sup>I<sub>15/2</sub> weak emission (at about 810 nm), which disappears in most matrices, was observed for LiYF<sub>4</sub> [4]. Because of the strong spin–orbit coupling ( $\zeta_{4f} \approx 2380 \text{ cm}^{-1}$ ) [5], the energy gaps between different <sup>2S+1</sup>L<sub>J</sub> levels are larger than 1000 cm<sup>-1</sup> in most cases. In addition, because of the small CF mixing, J remains a good quantum number. These show the convenience of CF simulation.

### 2. Experimental details

Polycrystalline powders of LaOX:0.005Er<sup>3+</sup> phosphors were prepared by a solid state reaction between corresponding RE oxides and ammonium halides under the protection

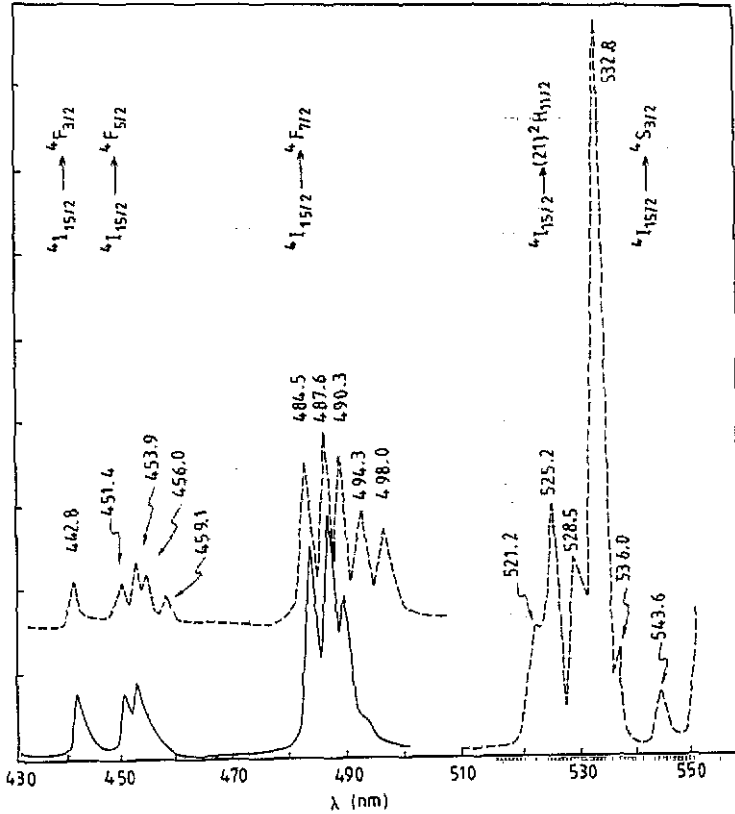


Figure 1. Part of the excitation spectrum of  $\text{LaOCl}:\text{Er}^{3+}$  at RT (---) and LNT (—) ( $\lambda_{\text{em}} = 551.5 \text{ nm}$ ).

of a reductive atmosphere of  $\text{N}_2$ -10%  $\text{H}_2$  or in the presence of carbon powders.  $\text{Er}_2\text{O}_3$  and  $\text{La}_2\text{O}_3$  of high purity (99.99% or higher) were products obtained from the Shanghai Chemical Plant. The samples prepared in a  $\text{N}_2$ - $\text{H}_2$  atmosphere emit with a higher luminosity. The fluorescence spectra were measured at room temperature (RT) and liquid-nitrogen temperature (LNT) with a Hitachi model 850 fluorescence spectrophotometer. Some of the results are shown in figures 1-3.

Figure 1 shows clearly that two more peaks appear in the  ${}^4\text{I}_{15/2} \rightarrow {}^4\text{F}_{5/2}$  and  ${}^4\text{I}_{15/2} \rightarrow {}^4\text{F}_{7/2}$  excitation bands at RT than at LNT. For  $\text{LaOCl}:\text{Er}^{3+}$ , these peaks are located at 456.0 and 459.1 nm and at 494.3 and 498.0 nm, respectively. This evident temperature effect not only shows the difference between the population numbers of the different Stark components of the  ${}^4\text{I}_{15/2}$  level but also provides evidence for the spectral analysis. This will be discussed in section 4.

The emission spectra of  $\text{LaOX}:\text{Er}^{3+}$  covers the whole visible region with the main peak between 530 and 560 nm ( ${}^4\text{S}_{3/2} \rightarrow {}^4\text{I}_{15/2}$  green emission, see figures 2 and 3). All the emission bands show considerable CF splitting. The appearance of the  ${}^4\text{I}_{9/2} \rightarrow {}^4\text{I}_{15/2}$  weak emission at about 810 nm indicates that the effective non-radiative transition from  ${}^4\text{F}_{9/2}$  to  ${}^4\text{I}_{9/2}$  greatly increases the population number of the  ${}^4\text{I}_{9/2}$  emitting level. It has been pointed out above that this emission band does not appear in most matrices.

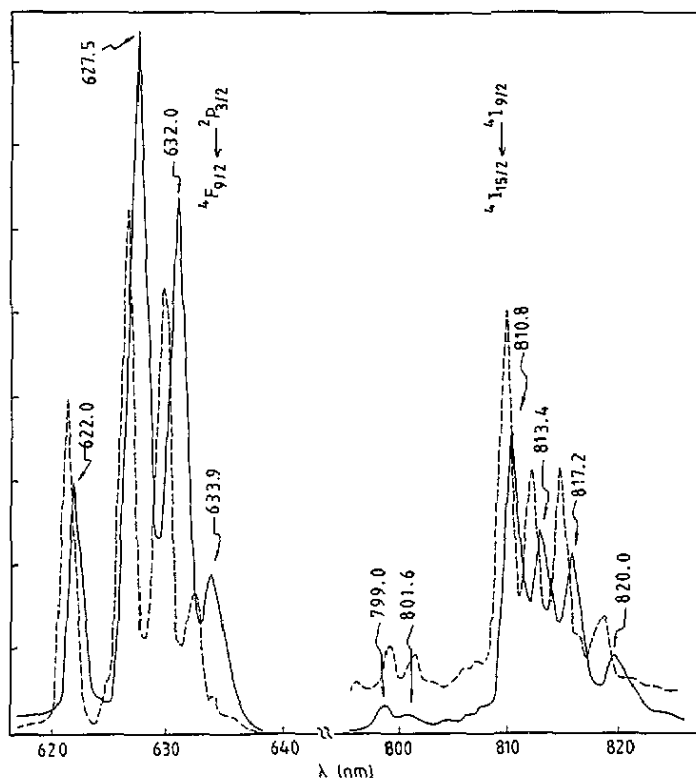


Figure 2. Emission spectra (620–820 nm) of LaOBr:Er<sup>3+</sup> (—) and LaOCl:Er<sup>3+</sup> (---) at LNT ( $\lambda_{\text{ex}} = 263$  nm).

### 3. Calculation of the DSCPCF perturbation energy of Er<sup>3+</sup> in LaOX

The energy Hamiltonian of Er<sup>3+</sup> in LaOX is  $\hat{H} = \hat{H}_0 + \hat{H}_{\text{CF}}$ , where  $\hat{H}_0$  represents the free-ion Hamiltonian including the spin-orbit coupling and  $\hat{H}_{\text{CF}}$  the CF perturbation potential operator. Because the deviation between the theoretically calculated free-ion energy level and the measured value is usually comparable with the CF perturbation, we prefer to take the measured eigenvalues of  $\hat{H}_0$ , which has been shown later in the middle of figure 5, as the start of the CF calculation.

The whole LaOX ( $X^- \equiv \text{Cl}^-, \text{Br}^-, \text{I}^-$ ) series has tetragonal crystal structure (space group,  $P_4/nmm$  ( $D_{2h}^2$ );  $Z = 2$ ) with layers of  $(\text{LaO})^{n+}$  complex cations alternating with halide layers (figure 4) [6–8]. Trace amount of Er<sup>3+</sup> ions in LaOX matrices are coordinated to four oxygen and five halide ligands with  $C_{4v}$  point site symmetry. In terms of the contribution to the CF effect on RE ions, the nine ligands can be classified into three equivalent series:

- |          |  |
|----------|--|
| series 1 | 4O ( $R_O, \Theta_O, \Phi_O$ )           |
| series 2 | 4X ( $R_X, \Theta_X, \Phi_X$ )           |
| series 3 | 1X' ( $R_{X'}, \Theta_{X'}, \Phi_{X'}$ ) |

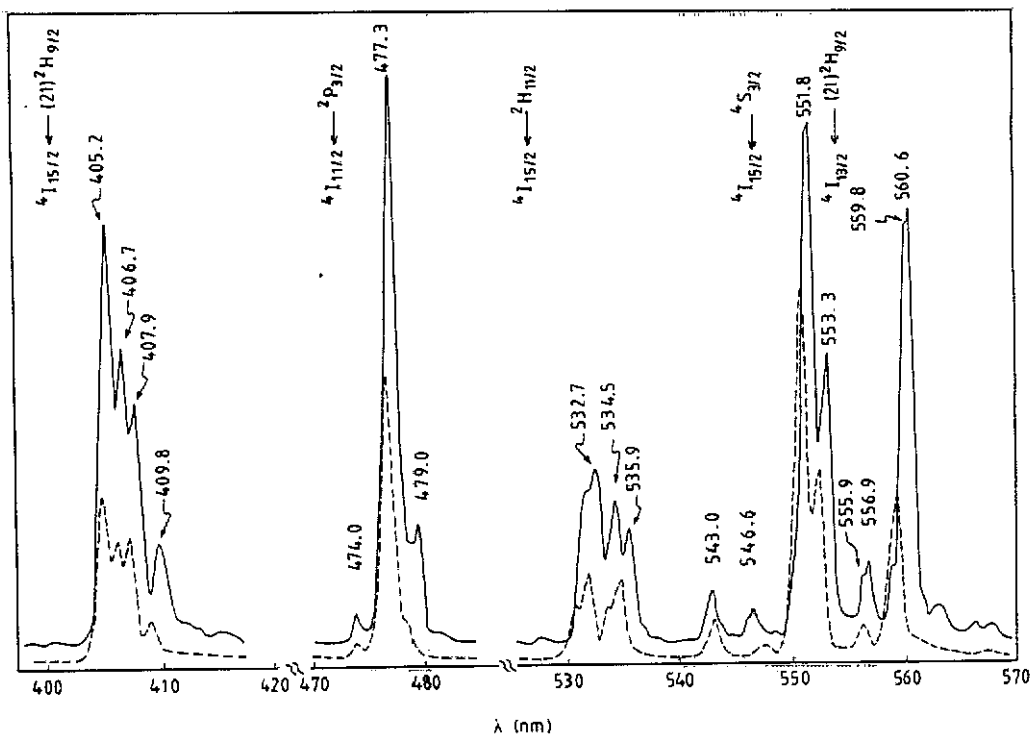


Figure 3. Emission spectra (400–570 nm) of LaOBr: Er<sup>3+</sup> (—) and LaOCl: Er<sup>3+</sup> (---) at LNT ( $\lambda_{exc} = 263$  nm).

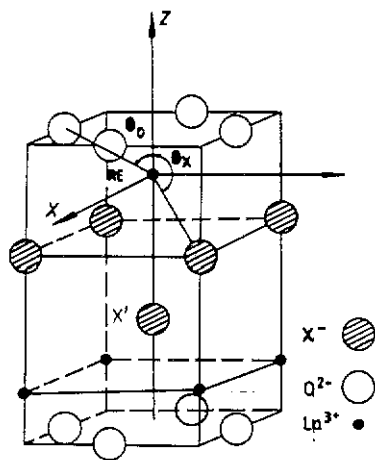


Figure 4. Unit cell of LaOX and coordinate system used in CF calculations.

in which  $\Phi_{O_j} = 0^\circ, 90^\circ, 180^\circ, 270^\circ$ ,  $\Phi_{X_j} = 45^\circ, 135^\circ, 225^\circ, 315^\circ$ ,  $\Phi_{X'} = 0^\circ$ , and  $R_j$  and  $\Theta_j$  are listed in table 1. The fact that the La–X and La–X' distances vary considerably while the La–O distance remains almost the same indicates that La–X and La–X' coordination may have a major effect on the variation in CF perturbation in the LaOX series. It should

**Table 1.** Spherical coordinates  $R_j$  and  $\Theta_j$ , and the effective charge  $Z_j^*$  and  $Q_j$  of the ligands in the LaOX:Er<sup>3+</sup> series ( $X^- \equiv \text{Cl}^-, \text{Br}^-$ ).

| Parameter used in calculations | LaOCl   |         |        | LaOBr  |         |        |
|--------------------------------|---------|---------|--------|--------|---------|--------|
|                                | 4O      | 4X      | 1X'    | 4O     | 4X      | 1X'    |
| $Z_{X_j}^*/e$                  | 3.105   | 3.850   | 3.505  | 3.200  | 3.763   | 3.371  |
| $O_{X_j}/e$                    | -1.600  | -0.706  | -0.700 | -1.650 | -0.750  | -0.750 |
| $R_j$ (Å)                      | 2.39    | 3.18    | 3.14   | 2.40   | 3.28    | 3.47   |
| $\Theta_j$ (deg)               | 59.5100 | 113.666 | 180    | 59.954 | 116.396 | 180    |

also be pointed out that X and X' are different halogen ligands because of their different distances to RE ions.

In a tetragonal perturbation field the CF Hamiltonian  $\hat{H}_{\text{CF}}$  is described by five non-zero  $B_m^k$  CF parameters:

$$\hat{H}_{\text{CF}} = B_0^2 C_0^2 + B_0^4 C_0^4 + B_4^4 (C_{-4}^4 + C_4^4) + B_0^6 C_0^6 + B_4^6 (C_{-4}^6 + C_4^6) \quad (1)$$

in which  $C_m^k = \sqrt{4\pi}/(2k+1) Y_m^k$ ,  $B_m^k = A_m^k \langle r^k \rangle$ .

From the viewpoint of the DSCPCF model [3], a complex unit  $\text{MX}_n$  can be considered as an entity in which its central ion M with effective nuclear charge  $Z_m^*$  is surrounded by  $n$  positive ligands with effective nuclear charge  $Z_{X_j}^*$  (the secondary-sphere coordination point charge) and  $n$  negative bond charges with magnitude  $q_j$  (which distribute along the M—X bonds and form the first-sphere coordination point charge). The magnitude of the bond charge  $q_j$  and its position  $r_j$  depend primarily on  $Z_m^*$  and  $Z_{X_j}^*$ , and can be calculated as follows:

$$\begin{aligned} q_j &= Z_m^* Z_{X_j}^* / (\sqrt{Z_m^*} + \sqrt{Z_{X_j}^*})^2 \\ r_j &= R_j \sqrt{Z_m^*} / (\sqrt{Z_m^*} + \sqrt{Z_{X_j}^*}) \end{aligned} \quad (2)$$

where  $R_j$  is the M—X bond length. The space distribution of the double-sphere coordination point charge possesses the point group symmetry of the complex and satisfies the Feynman force equilibrium requirements. In this model the lattice sum  $A_m^k$  can be represented as the contributions from  $Z_{X_j}^*$  and  $q_j$ :

$$A_m^k = \sum_j \left( \frac{q_j}{r_j^{k+1}} - \frac{Z_{X_j}^*}{R_j^{k+1}} \right) C_m^{k*}(\Theta_j, \Phi_j). \quad (3)$$

In the simulation,  $M \equiv \text{RE}$ ,  $Z_m^* = 18.10 + 0.65(N-1)$  [9, 10] and  $Z_j^*$  are the only parameters which can be adjusted in the CF simulation.

By applying equation (3) in figure 4, the specific forms of  $A_m^k$  are as follows:

$$\begin{aligned} A_0^2 &= 2[(3 \cos^2 \Theta_0 - 1)(q_0/r_0^3 - Z_0^*/R_0^3) + (3 \cos^2 \Theta_X - 1) \\ &\quad \times (q_X/r_X^3 - Z_X^*/R_X^3)] + (q_{X'}/r_{X'}^3 - Z_{X'}^*/R_{X'}^3) \\ A_0^4 &= \frac{1}{2}[(35 \cos^4 \Theta_0 - 30 \cos^2 \Theta_0 + 3)(q_0/r_0^5 - Z_0^*/R_0^5) + (35 \cos^4 \Theta_X \\ &\quad - 30 \cos^2 \Theta_X + 3)(q_X/r_X^5 - Z_X^*/R_X^5)] + (q_{X'}/r_{X'}^5 - Z_{X'}^*/R_{X'}^5) \\ A_0^6 &= \frac{1}{4}[(231 \cos^6 \Theta_0 - 315 \cos^4 \Theta_0 + 105 \cos^2 \Theta_0 - 5)(q_0/r_0^7 - Z_0^*/R_0^7) \\ &\quad + (231 \cos^4 \Theta_X - 315 \cos^2 \Theta_X + 105 \cos^2 \Theta_X - 5)(q_X/r_X^7 - Z_X^*/R_X^7)] \\ &\quad + (q_{X'}/r_{X'}^7 - Z_{X'}^*/R_{X'}^7) \end{aligned} \quad (4)$$

$$A_4^4 = (\sqrt{70}/4)[\sin^4 \Theta_O (q_O/r_O^5 - Z_O^*/R_O^5) - \sin^4 \Theta_X (q_X/r_X^5 - Z_X^*/R_X^5)]$$

$$A_4^6 = (3\sqrt{14}/8)[\sin^4 \Theta_O (11 \cos^2 \Theta_O - 1)(q_O/r_O^7 - Z_O^*/R_O^7) - \sin^4 \Theta_X (11 \cos^2 \Theta_X - 1)(q_X/r_X^7 - Z_X^*/R_X^7)].$$

The basis function for irreducible representation of the tetragonal groups is the linear transformation of the  $L$ - $S$  coupling wavefunction:

$$|J\Gamma p_\rho\rangle = \sum_M S_{M,\rho}^{\Gamma} |JM\rangle \quad (5)$$

in which  $J$ ,  $\Gamma$  and  $P$  represent the irreducible representations of the  $R(3)^*$ ,  $O^*$  and  $D_4^*$  (which is isomorphous with  $C_{4v}^*$ ) groups, respectively, and  $\rho$  the row label of the  $P$  representation. The CF perturbation matrix elements can be derived from the above equation as follows:

$$\langle J\Gamma p | \hat{H}_c | J'\Gamma' p' \rangle = \delta_{pp'} \sum_{k,m} F_m^k T_m^k \quad (6)$$

in which  $T_0^2 = aB_0^2$ ,  $T_0^4 = bB_0^4$ ,  $T_0^6 = cB_0^6$ ,  $T_4^4 = \sqrt{70} bB_4^4$  and  $T_4^6 = \sqrt{14} cB_4^6$ . The calculation procedure above has been programmed.

The values of the radial integrals  $\langle r^k \rangle$  are as follows [10]:  $\langle r^2 \rangle = 0.666a_0^2$ ,  $\langle r^4 \rangle = 1.126a_0^4$  and  $\langle r^6 \rangle = 3.978a_0^6$ . The simulated values of  $Z_{X,Y}^*$  are listed in table 1. The corresponding CF perturbation energy levels of  $\text{Er}^{3+}$  in the LaOX series are shown in figure 5. As a comparison, the calculated results of the point-charge electrostatic model (PCEM) are shown in figure 5 too. The numbers in parentheses in the middle of figure 5 are the free-ion energy levels of  $\text{Er}^{3+}$  in the LaOCl matrix. It should be pointed out that, because the two energy levels  ${}^4F_{3/2}$  and  ${}^4F_{5/2}$  are close to each other,  $J$  mixing between them should be taken into account in the CF calculation. The results are shown in the upper right of the corresponding levels in figure 5. This correction is smaller than  $15 \text{ cm}^{-1}$ .

#### 4. Theoretical assignments of the fluorescence spectra of $\text{LaOX}:\text{Er}^{3+}$

Because of the Kramers degeneracy, the  $\text{Er}^{3+}$  ion has only two kinds of Stark component  $\varepsilon'$  and  $\varepsilon''$  in the  $C_{4v}^*$  CF. According to the group theory selection rule in  $C_{4v}^*$  site symmetry, transitions between any different Stark components are allowed. Figures 6–8 show part of the assignment of the fluorescence spectra of  $\text{LaOX}:\text{Er}^{3+}$  based on the DSCPCF model. The calculated lines agree well with the measured lines.

According to the assignment in figure 6, it is easy to explain the temperature effect on  ${}^4I_{15/2} \rightarrow {}^4F_{5/2}$  and  ${}^4I_{15/2} \rightarrow {}^4F_{7/2}$  excitation bands in figure 1. For the  ${}^4I_{15/2}$  level, the Stark components  $(11)\varepsilon''$ , and so on  $(3)\varepsilon''$ ,  $(7)\varepsilon'$  with higher energies possess a non-negligible population number at RT (0.299 or higher; see the population number shown on the right of figure 6), the excitation transitions from these Stark components appear in the excitation spectra, while at LNT the population number of these components becomes very small (0.144 or less), and therefore the corresponding emission lines disappear in the spectra.

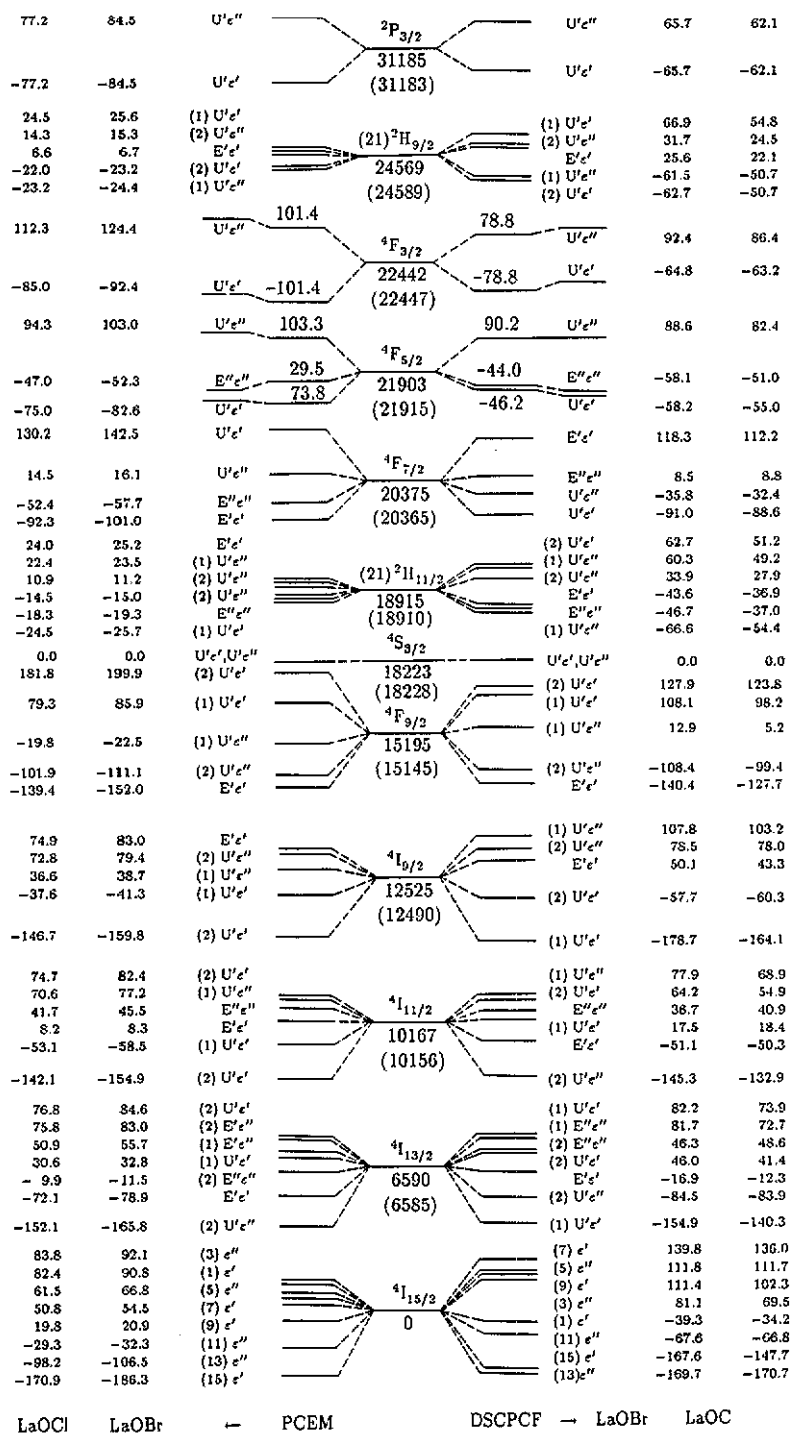


Figure 5. CF perturbation energy levels of LaOX:Er<sup>3+</sup> (X<sup>-</sup> ≡ Cl<sup>-</sup>, Br<sup>-</sup>) phosphors.

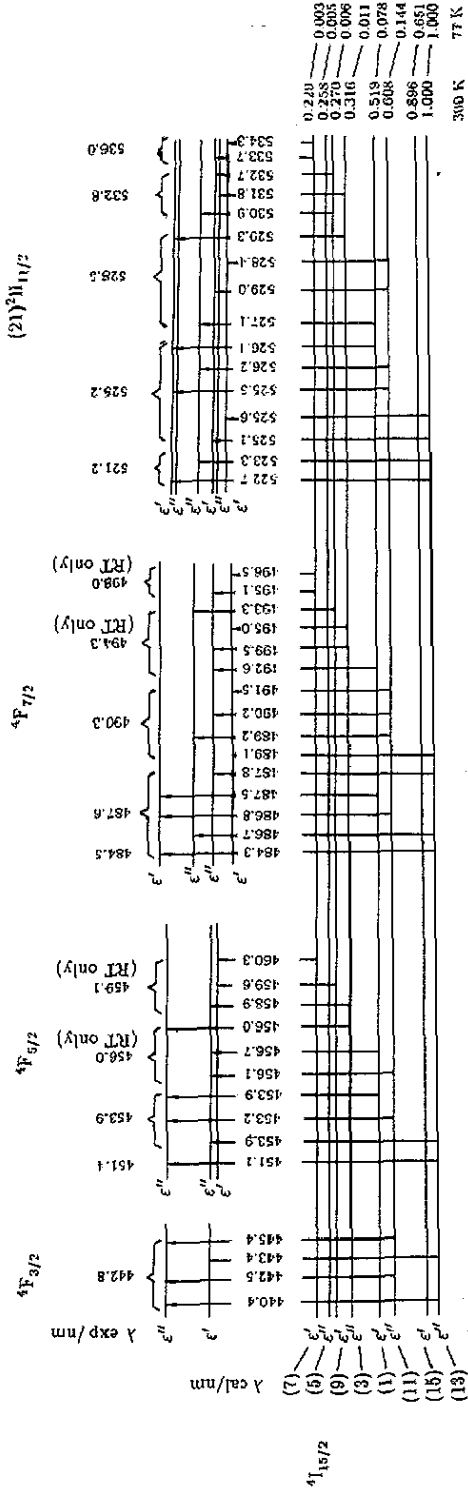


Figure 6. Assignments of the excitation spectrum of  $LaOCl:Er^{3+}$  transitions:  $4I_{15/2} \rightarrow 4F_J (J = 3/2, 5/2, 7/2)$ ,  $4I_{15/2} \rightarrow (21)2H_{11/2}$ .

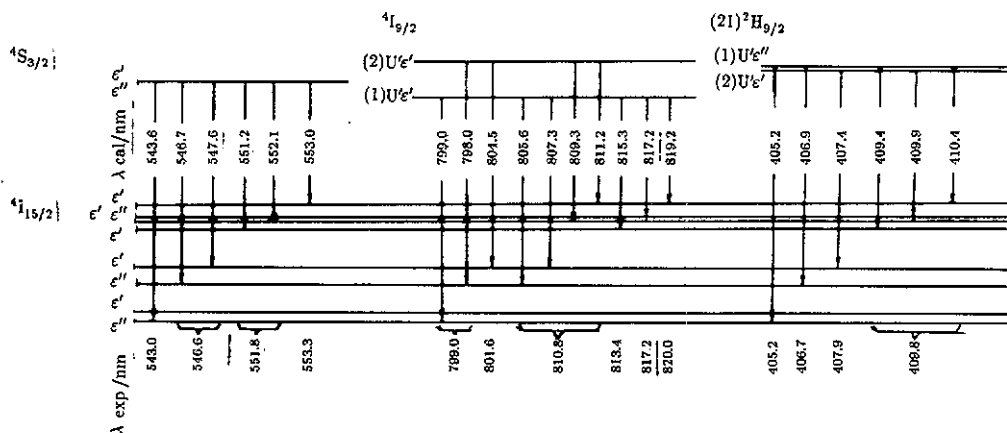


Figure 7. Assignments of the emission spectrum of LaOBr:Er<sup>3+</sup> transitions: (21)<sup>2</sup>H<sub>9/2</sub> → <sup>4</sup>I<sub>15/2</sub>, <sup>4</sup>I<sub>9/2</sub> → <sup>4</sup>I<sub>15/2</sub> and <sup>4</sup>S<sub>3/2</sub> → <sup>4</sup>I<sub>15/2</sub>.

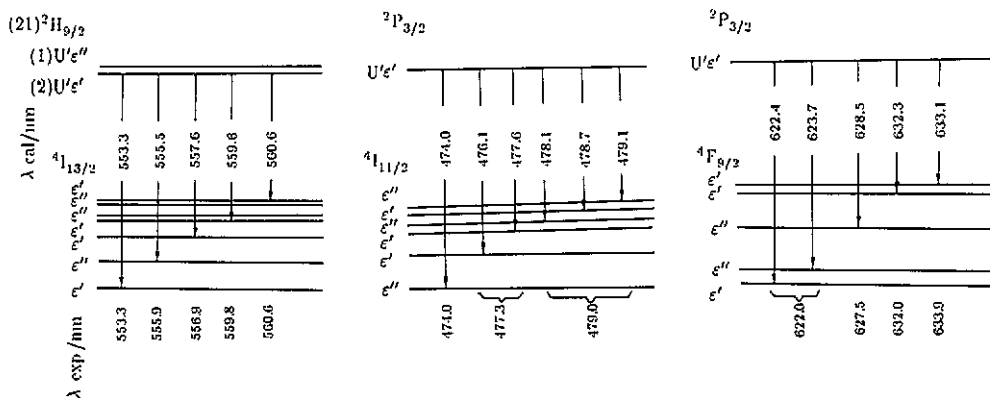


Figure 8. Assignments of the emission spectrum of LaOBr:Er<sup>3+</sup> transitions: (21)<sup>2</sup>H<sub>9/2</sub> → <sup>4</sup>I<sub>13/2</sub>, <sup>2</sup>P<sub>3/2</sub> → <sup>4</sup>I<sub>11/2</sub> and <sup>2</sup>P<sub>3/2</sub> → <sup>4</sup>F<sub>9/2</sub>.

### 5. Discussion and conclusion

Although there have been several models describing the crystal-field effect, such as the angular overlap model, the polarization model and the superposition model [11, 12], it is proper to compare the DSCPCF model with the PCEM model considering their physical characteristics.

As Hüfner [11] pointed out earlier, the calculations of  $B_m^k$  performed with the point-charge model show that the results were mostly too large for  $k = 2$  terms, of the right magnitude for  $k = 4$  terms, and an order of magnitude too small for the  $k = 6$  terms. Some modifications have been made to overcome the shortcomings. The introduction of the shielding effect of the outer 5S<sup>2</sup> and 5P<sup>6</sup> shells into this model by Burns *et al* [13] largely rectify the discrepancies in  $B_m^2$ . The largest discrepancy remained in  $B_m^6$ . Leavitt *et al* [14] modified this model in another way. They corrected  $r$  to  $r/\tau$  ( $\tau \approx 0.75$ ) based on the consideration that the Hartree-Fock radial functions do not give an adequate

Table 2. The calculated CF parameters  $B_m^k$  for LaOX:Er<sup>3+</sup> and LaOX:Eu<sup>3+</sup>. All values are in cm<sup>-1</sup>.

| $B_m^k$ | LaOCI:Er <sup>3+</sup> |      |         |         | LaOBr:Er <sup>3+</sup> |      |         |         | LaOCI:Eu <sup>3+</sup> |       |         |         | LaOBr:Eu <sup>3+</sup> |       |         |         | LaOI:Eu <sup>3+</sup> |       |         |         |
|---------|------------------------|------|---------|---------|------------------------|------|---------|---------|------------------------|-------|---------|---------|------------------------|-------|---------|---------|-----------------------|-------|---------|---------|
|         | DSCPCF                 | PCEM | $R_m^k$ | $R_m^k$ | DSCPCF                 | PCEM | $R_m^k$ | $R_m^k$ | DSCPCF                 | PCEM  | $R_m^k$ | $R_m^k$ | DSCPCF                 | PCEM  | $R_m^k$ | $R_m^k$ | DSCPCF                | PCEM  | $R_m^k$ | $R_m^k$ |
| $B_0^0$ | 931                    | 1157 | 0.80    | 0.78    | 985                    | 1268 | 0.78    | 0.71    | -1123                  | -1586 | 0.71    | 0.81    | -1263                  | -1749 | 0.72    | 0.81    | -1263                 | -1749 | 0.72    | 0.81    |
| $B_2^0$ | 637                    | 234  | 2.72    | 3.05    | 753                    | 247  | 3.05    | 2.51    | -960                   | -382  | 2.51    | 3.21    | -1371                  | -439  | 3.12    | 3.21    | -1371                 | -439  | 3.12    | 3.21    |
| $B_4^0$ | -394                   | -210 | 1.88    | 2.27    | -504                   | -222 | 2.27    | 1.84    | 601                    | 326   | 1.84    | 2.24    | 734                    | 383   | 1.92    | 2.24    | 734                   | 383   | 1.92    | 2.24    |
| $B_6^0$ | -428                   | -51  | 8.39    | 8.00    | -408                   | -51  | 8.00    | 7.93    | 825                    | 104   | 7.93    | 8.90    | 653                    | 98    | 6.67    | 8.90    | 653                   | 98    | 6.67    | 8.90    |
| $B_8^0$ | -319                   | -50  | 6.38    | 6.29    | -317                   | -49  | 6.29    | 6.21    | 615                    | 99    | 6.21    | 6.90    | 525                    | 102   | 5.15    | 6.90    | 525                   | 102   | 5.15    | 6.90    |

approximation to the true radial charge distribution. According to this assumption,  $B_m^4$  and  $B_m^6$  will be increased by 3.2 and 5.6 times, respectively. We believe that both of the above modifications paid too much attention to the corrections of the central ion parameters with too little consideration of the coordinate bonding effects of the ligands and therefore cannot represent the true charge distribution around the central ion. This is the problem of the point-charge model itself. From the viewpoint of the bonding effect, there must be charge 'accumulation' to a certain degree along the central ion-ligand bonds. This effect is at least qualitatively reflected by the bond charge  $q$  in the DSCPCF model. The correction of the DSCPCF model to the PCEM model is reasonably described by the ratios of the  $B_m^k$  parameters in the two models. Let  $R_m^k = B_m^k(\text{DSCPCF})/B_m^k(\text{PCEM})$ . Table 2 shows clearly that the DSCPCF model makes  $B_m^2$  decrease slightly and  $B_m^4$  and especially  $B_m^6$  increase greatly. For example, for LaOX:Er<sup>3+</sup>,  $R_0^2 \approx 0.8$ ,  $R_m^4 = 1.8\text{--}3.0$  and  $R_m^6 = 6.2\text{--}8.3$ . A similar correction exists in table 2 for LaOX:Eu<sup>3+</sup> and other RE complexes [2, 10]. This correction to  $B_m^4$  and  $B_m^6$  parameters with the DSCPCF model is similar to that with the modification of  $\langle r^k \rangle$  by Leavitt *et al* [14]. Sophisticated calculations have shown that the excited 5d states contribute the most to the bonding effect between the RE ion and its ligands while the 4f orbitals contribute very little [15]. It is reasonable to keep the free-ion Hartree-Fock  $\langle r^k \rangle$  of inner 4f orbitals fixed in CF calculations.

The CF parameters  $B_m^k$  for the same RE ion in table 2 show an increasing trend along the LaOX series ( $X^- \equiv \text{Cl}^-, \text{Br}^-, \text{I}^-$ ). This kind of evolution could be related to increases in both the ionic radius and the electronegativity of the  $X^-$  host anions, which naturally led to the 'covalency' effect for LaOBr and especially for LaOI. It also should be noted that the energy levels of the charge transfer state of RE ions show a decreasing tendency along the LaOX series [2]. The facts above indicate that the bonding effect between the RE ion and its ligands with lower electronegativity in crystals is non-negligible. In such systems, the DSCPCF model shows its advantages, especially for the  $^{2S+1}L_J$  terms with large  $J$ -values and some terms involved in supersensitive transitions of RE ions.

## References

- [1] Hölsä J and Porcher P 1981 *J. Chem. Phys.* **75** 2108; 1982 *J. Chem. Phys.* **76** 2790
- [2] Yang Pin, Li Sidian and Wang Yuekui 1990 *Acta Chim. Sinica* at press
- [3] Yang Pin and Li Lemin 1981 *Kexue Tongbao* **26** 865
- [4] Brenier A, Moncorge R and Pedrini C 1986 *J. Less-Common Met.* **126** 203, 283
- [5] Carnall W T, Fields P R and Rajnak K 1968 *J. Chem. Phys.* **49** 4424
- [6] Blasse G and Bril A 1967 *J. Chem. Phys.* **46** 2579
- [7] Templeton D H and Dauben C H 1953 *J. Am. Chem. Soc.* **71** 6069
- [8] Mayer I, Zolotov S and Kassierer F 1965 *Inorg. Chem.* **4** 1637
- [9] Burns G 1964 *J. Chem. Phys.* **41** 1521
- [10] Yang Pin and Wang Yuekui 1987 *Sci. Sinica B* **30** 907
- [11] Hüfner S 1978 *Optical Spectra of Transparent Rare Earth Compounds* (New York: Academic)
- [12] Gschneidner K A Jr and Eyring L 1982 *Handbook on the Physics and Chemistry of Rare Earths* vol 5 (Amsterdam: North-Holland) p 485
- [13] Burns G 1962 *Phys. Rev.* **128** 2121
- [14] Leavitt R P, Morrison C A and Wortman D E 1975 *Harry Diamond Laboratories Report TR-1673*; 1975 *National Technical Information Services Report* 017849
- [15] Ren Jingqing, Li Lemin, Wang Xiuzheng and Xu Guangxian 1982 *J. Beijing Univ. (Natural Section)* **3** 30, 49